Journal of Power Technologies 105 (1) (2025) 1 -- 14

Thermal-hydraulic design of a small passively liquid-metal-cooled reactor

Roman Thiele ✉, Henryk Anglart

KTH Royal Institute of Technology, Nuclear Reactor Technology of the department of Physics,
✉ romant@kth.se

Abstract

The influence of bypass flow size and thermal shielding on the overall performance of a small pool-type liquid-metal-cooled reactor are investigated through the use of 3D computational fluid dynamics. 1/4 of the reactor is modeled using a porous media approach for small-detail domains, such as the core and the heat exchangers, and a full conjugate heat transfer approach for all relevant walls. Through the introduction of thermal shielding on the internal wall and an optimal bypass flow based on the ratio of pressure drops over the core and heat exchangers, most of the critical design parameters are in good agreement. The results show that for a well-functioning design the pressure drops of the core and the heat exchanger should be close in value, which can be achieved by selecting the right bypass flow.

Introduction

The next generation of nuclear reactors, the so-called GEN IV, builds on several fundamentally different cooling concepts and liquids, such as supercritical water, gas and liquid metal cooled reactors. One of the most promising concepts is the liquid-metal-cooled reactor, which includes sodium and lead-bismuth-eutectic (LBE) [1]. Lead is not just chemically inert but also exhibits a very high boiling point of around 2023 K, which makes it a low-accident-probability coolant [2]. Together with some other favorable thermophysical traits, such as high thermal conductivity and a large absolute density difference due to temperature make this coolant a perfect candidate for passive cooling in accident as well as during operating conditions.

Prior to the commercial deployment of GEN IV reactors, different aspects should be studied, such as training and educating of new personnel and nuclear engineering students. This aspect has been identified by Wallenius et al. [3] who proposed the ELECTRA concepts.

Literature study

Lately, multiple notable projects have developed and refined reactor concepts using liquid lead/LBE as coolant. These projects include ELSY, SSTAR, ALFRED and MYRRHA/FASTEF [4-7].

The ELSY concept is a $600 MW_e$ pool-type critical reactor, which is actively cooled with pumps during operation. However, ELSY relies on passive heat removal in accidents and abnormal conditions, where pump power is not available [6]. Bandini et al. [8] successfully demonstrated the passive cooling capabilities of ELSY using the system code RELAP5. System codes give a quick and good overview of certain capabilities, especially for large systems, however, more insight can be gained through the use of 3D computational fluid dynamics (CFD).

Smith et al. [9] designed SSTAR as a small transportable reactor, which can last unsupervised for up to 30 years and is very proliferation resistant. Its design is similar to ELECTRA's design by Wallenius et al. [3] which also uses just one large fuel assembly and relies on natural convection for heat removal in the primary circuit. The difference is the much larger thermal power of 45MW_{th}.

An interesting concept combining two reactors in one is the 110-MW-power MYRRHA/FASTEF design. In its first phase, it will run as a sub-critical accelerator driven system (ADS), which employs a proton accelerator in combination with a spallation source to produce the missing neutrons and achieve sustainable neutron economy Abderrahim et al. [10]. During the second phase, the reactor will run in self-sustained critical condition. In both phases, MYRRHA relies on active cooling during normal operation and passive natural-convection-driven cooling during accident and abnormal conditions. Recently, Castelliti and Baeten [7] performed a safety analysis using RELAP5 and Vanderhaegen et al. [11] performed a detailed analysis using a commercial CFD code. They demonstrated that a full reactor analysis with CFD is feasible and leads to detailed insights into the flow path during natural-convection cooling and thermal-hydraulic behavior of the reactor. They modeled the fine detail parts of the reactor, such as the core, using a porous media approach. Other groups also performed full reactor CFD analyses and investigations similar to the one in this work. Abanades and Pena [12] analyzed the Ansaldo ADS reactor called EADF in a 2D-symmetric CFD approach, where they replaced the core, the dummy assemblies and the heat exchanger domains with porous media domains to reduce the global number of cells dramatically. The main driving force of the coolant in EADF is natural convection. The use of this 2D-approach made it possible for them to analyze and optimize the flow path in the reactor and channel more flow through the core instead of the dummy assemblies.

Shibahara et al. [13] used the commercial code ANSYS Fluent to perform a highly detailed study of the natural convection flow phenomena in the MONJU reactor's upper plenum after a turbine trip. They used a high-resolution tetrahedral mesh for the coolant domain in conjunction with a porous zone, which represents the honeycomb structure at the outlet of the core. Different steady-state and transient computations were performed, and the transient results are in good agreement with the experimental results for the first 250 s of the transient. The results diverge from one another at this point. However, the error can be traced back to the inlet boundary conditions of the computations, which do not reliably reproduce the fluctuating mass flow after a pump trip.

The small passively cooled reactor

In contrast to many of the aforementioned reactor concepts, of which many use active cooling in operating mode and only passive cooling when accidents occur or during shutdown scenarios, the reactor investigated in this paper uses passive cooling at all times. A full description of the reactor concept ELECTRA can be found in Wallenius et al. [3] The design consists of one large fuel assembly, with a thermal power of approximately 0.5MW. The power in the core, startup and shutdown are controlled through reactivity control drums situated around the core. The system heat removal is achieved through eight heat exchangers similar to the ones in the ALFRED concept [18]. The reactor vessel's overall size is approximately 1x2.5 m and the core is only 0.48m high and the flat-to-flat distance of the hexagonal assembly is 0.3m.

Recent investigations of ELECTRA include one by Suvdantsetseg [14]. The author used the 1D system code SAS4A/SASSYS1 for coupled thermal-hydraulic-neutronic computations,

where the neutronic code was Serpent. Pumps were used to model the natural-convection driving force in SAS4A/SASSYS-1, where in reality this driving force stems from the temperature difference between the core and the heat exchangers. Due to the system code limitations, 3D effects due to buoyancy were not accounted for, however some overall qualitative insight into the system was gained.

These 3D effects were captured in previous work, which used the commercial CFD code ANSYS CFX to analyze the flow path and natural convection behavior in ELECTRA [15, 16]. Several hot spots were found in the reactor. The studies also found that the influence of the heat transfer between the hot and cold leg (flow shroud) in the primary system cannot be neglected and if necessary, needs to be dealt with through design changes.

Methods

Modeling a 397-pin fuel rod bundle using the CFD approach can be challenging and together with the heat exchangers, the number of cells needed to fully model the present geometry of a small-scale training reactor would lead to exorbitant computational costs and would be unfeasible. As Sha [17] explains, there are different approximations for sub-channel modeling, such as sub-channel analysis and the porous media approach. The former one has large drawbacks, such as that the sub-channel analysis mostly employs the dominant flow direction (information loss) and interfacing between the sub-channel analysis and the CFD code is cumbersome and complex. Even in the porous media approach some need for modeling of heat transfer and pressure drop remains. Through an anisotropic modeling approach, a difference in pressure drop between the main flow direction (along the rod bundle) and the transverse direction (perpendicular to the rod bundle) can be achieved. Interfacing between the different domains in ANSYS CFX is readily available through the generalized grid interfaces [18]. This is the reason to use a porous media approach for the heat exchangers domains and for the core domains.

The mesh of one quarter of the geometry shown in Figure 1 consists of 3.7M cells, of which the largest part is the tetrahedra in the very complex fluid geometry. The core, the heat exchangers, the wrappers around the core and heat exchangers and the wall separating the hot leg from the cold leg (flow shroud) employ purely hexahedral meshes in order to reduce the number of cells and increase the accuracy in these domains. Tet-meshes have been successfully employed for similar natural convection computations by Shibahara et al. [13]. Only one quarter of the geometry is modeled, helping to increase stability in the computations and increase the resolution of the model, but at the same time keeping the total number of cells at a minimum. Along the walls boundary layer cells are introduced to assure that a maximum wall distance of $y^+ < 150$ is achieved at all points in the domain.

Thermal barrier for the flow shroud

Previous studies have found the need to include conjugate heat transfer in the computations in order to model the heat losses from the hot to the cold leg [16]. Therefore, the present study includes conjugate heat transfer in the most critical internal structures, such as the wrappers around the core and the heat exchangers and the flow shroud.

The wall heat transfer between the hot and cold leg is very large and therefore decreases the achievable pressure drop dramatically. This pressure drop has to be overcome by the buoyancy pressure, which can be estimated by

$$\Delta P_p = \Delta\rho\delta L g \,, \qquad (1)$$

where $\Delta\rho$ is the density difference between the core and the HX due to temperature and g is the gravitational acceleration. The distance between the core and HX's is given by ΔL.

One way of increasing the achievable pressure is by increasing the density difference while keeping the geometry the same. Minimizing the heat losses through the flow shroud can be achieved by a method found in the turbine industry. On the walls of the flow shroud we introduce Zirconia coating, which is also used on turbine blades as a protective thermal barrier coating (TBC) to protect them from the hot flue gases [19, 20]. We chose Zirconia based coatings, because they achieve thermal conductivities of down to 1.6W/m/K and a thickness of up to 600µm. The addition of 600 µm Zirconia-based TBC to both sides of the wall decreases the heat flux through the wall by about 50%.

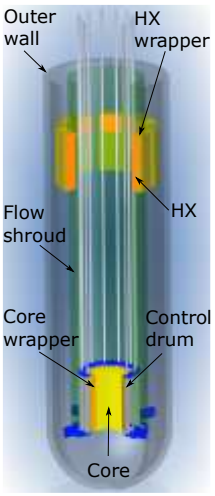

Figure 1: Modeled geometry of the reactor.

Numerical methods

The computations are carried out using Reynolds averaged Navier-Stokes (RANS) equation for flow and heat transfer in the fluid domain and for the fluid side in the porous domains [21]

$$\frac{\partial(\rho U_j)}{\partial t}+\frac{\partial(\rho U_i U_j)}{\partial x_j}=-\frac{\partial p}{\partial x_i}+\frac{\partial}{\partial x_j}\left(\tau_{ij}-\rho\overline{u_i u_j}\right)+\rho g_i+S_M, \quad (2)$$

where U_i is the velocity vector, ρ the density of the fluid, τ_{ij} the shear stress and S_M a source/sink term, which in our case is used to simulate the fluid's behavior in the porous media domains and is given in Eq. (9). A so-called full buoyancy model is used. The buoyancy forces are directly calculated from the density gradient within the fluid. The equations are closed through modeling of the Reynolds stresses, $u_i u_j$, using the k-ω-SST model eddy-viscosity model [22]. In the fluid domain the turbulence production and dissipation are influenced by the complex geometry and by buoyancy. Ansys [18] suggests using curvature compensation [23] and turbulent production due to buoyancy.
All wall boundaries make use of adaptable wall function, which works in a large range of y^+, which is expected with this kind of geometry [16].

The RANS temperature equation is given by [21]

$$\frac{\partial T}{\partial t}+\frac{\partial}{\partial x_j}\left(T U_j\right)=\frac{\partial}{\partial x_j}\left(\alpha\frac{\partial T}{\partial x_j}-\overline{u_j\theta}\right) \quad (3)$$

where α and T are the fluid's thermal diffusivity and temperature, respectively.

The turbulent heat fluxes, $u_j\theta$ are closed using the Reynolds analogy with a constant turbulent Prandtl number of 0.9. We know that using the Reynolds analogy together with RANS computations in liquid metals can be problematic due to a separation of scales between the thermal and velocity field, especially in the boundary layers Grotzbach [24]. However, in the present computations, heated boundary layers are avoided through porous-media modeling in the main regions of heat transfer from a wall to the fluid. A similar method has been successfully employed by Chen et al. [25].
In the solid domain a simple conduction equation is used to compute the temperature distribution,

where the subscript s denotes the solid phase. Balance between the solid and fluid domain is

achieved through heat flux conservation at the domain interface.

The material properties for stainless steel, which is used in all solid domains and on the solid side of the porous domain is taken from Leibowitz and Blomquist [26]. Conduction is kept at 20W/m/K. Material properties for the lead coolant are fully variable with temperature and are taken from [2].

$$(\rho c_{p,s})\frac{\partial T_s}{\partial t} - \nabla \cdot (\lambda_s \nabla T_s) = 0 \qquad (4)$$

Heat transfer in porous media

The heat transfer equations for the porous media make use of the local non-equilibrium of the temperature between the porous material (the core and heat exchangers) and the fluid flowing through the porous material. The heat transfer between the solid and the fluid is achieved by adding a source to the solid (Eq. (5)) and liquid phase heat equation (Eq. (6)) Nield and Bejan [27]),

$$\rho c_{p,s}(1-\varphi)\frac{\partial T_s}{\partial t} = (1-\varphi)\nabla \cdot (\lambda_s \nabla T_s) + h(T_f - T_s) \qquad (5)$$

$$\varphi(\rho c_p)_f \frac{\partial T_f}{\partial t} + (\rho c_p)_f \mathbf{u} \cdot \nabla T_f = \varphi \nabla \cdot (\lambda_f \nabla T_f) + h(T_s - T_f) \qquad (6)$$

where the subscripts s and f represent the different quantities and properties of the solid and fluid phase, respectively. The fluid-only properties are the density, ρ, and the specific heat capacity at constant pressure, c_p. The volume fraction of the fluid phase is given by ϕ and λ is the conductivity in the respective phase.

The heat transfer coefficient (HTC), h, is calculated by

$$h = a_{fs} h^* , \qquad (7)$$

where a_{fs} is the specific surface area (area per volume) through which heat transfer occurs. The HTC, h^*, is calculated from the Subbotin Nusselt number correlation for wire-wrapped rod bundles, which according to Mikityuk [28] works very well for this kind of conditions encountered in the present investigation, namely low-Reynolds-number flow in a tight rod bundle.

$$Nu = \frac{h^* D_h}{\lambda_s} = 0.58\left(\frac{2\sqrt{3}}{\pi}\left(\frac{p}{d}\right)^2 - 1\right)^{0.55} Pe^{0.45} \qquad (8)$$

In Eq. (8) p/d is the pitch-to-diameter ratio of the bundle, D_h is the hydraulic diameter of the bundle and $Pe = RePr$ is the temperature and flow dependent Peclet number. The Nusselt number correlation is valid for pitch-to-diameter ratios between 1.1 and 1.5 and a Peclet number range of 80 to 4000.

One of the goals of this investigation is to find the hot spots in the core and eliminate these. A detailed representation of the heat distribution is needed to achieve this goal. Suvdantsetseg et al. [29] carried out core design computations with a Monte-Carlo code, which resulted in the core power distribution shown in Figure 2.

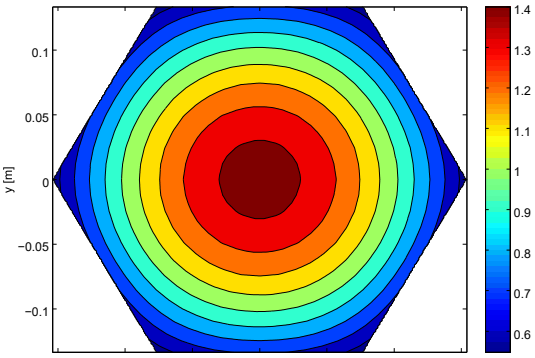

Figure 2: Normalized radial power profile of the reactor core from Suvdantsetseg et al. [26].

Pressure drop in porous media

The pressure drop in the porous-media domains is modeled using the Darcy-Forchheimer law for pressure drops in porous media Nield and Bejan [27],

$$\nabla P = -\frac{\mu}{K_{lin}}\mathbf{u} - c_F K^{-1/2}\rho_f|\mathbf{u}|\mathbf{u} = S_M\,, \qquad (9)$$

which we insert into the RANS equations as a source term in the porous domains. It is related to the friction factor by

$$\frac{f_{fric}}{D_h}0.5\rho u_i^2 = \nabla P\,, \qquad (10)$$

The coefficients for the linear and quadratic part of eq. (9) are calculated by translating a correlation friction coefficient for wired rod bundles into linear and quadratic coefficients through Reynolds number dependency. We used the friction coefficient correlation by Rehme [30], which according to a large comparison study by Bubelis and Schikorr [31] is the most suited correlation for our problem. We find the coefficients $1/K_{lin} = 8.1066 \cdot 10^6\,\mathrm{m}^{-1}$ and $2 \cdot c_F K^{-1/2} = 81.6352\,\mathrm{m}^{-2}$ for the linear and quadratic term, respectively, by fitting a quadratic curve to the correlation with respect to velocity. This methods allows the pressure drop to be temperature dependent through the variability of μ and ρ. The method has been tested in CFX with data
for tube bundles [30] and the results are generally in good agreement over the range of expected Reynolds numbers as shown in Figure 3.

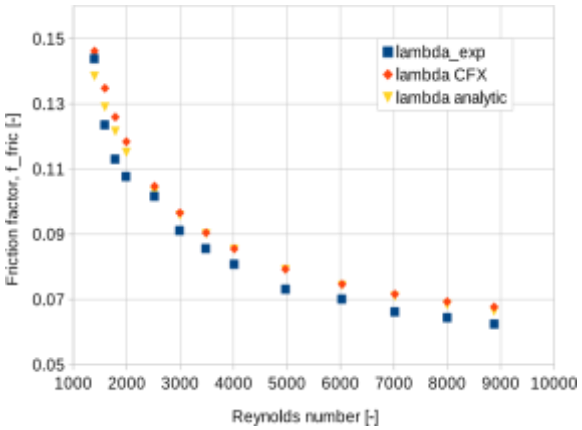

Figure 3: Results for CFX and analytical computations compared to experimental data from Rehme [31] for a 61-rod bundle with a 100-mm wire pitch

Boundary conditions

In pool-type reactors, the upper plenum is filled with an inert gas, however, modeling two-phase flow makes a model unnecessarily complex. Therefore, we model the upper surface of the reactor as an adiabatic boundary for the temperature and use full slip for the velocity. For the kind of computations carried out here, namely steady state behavior of the reactor, these kind of boundary conditions are sufficient. For violent transients, where the free surface in the reactor vessel might move this modeling approach is not valid.
At all other walls, the velocity boundary conditions is set to no slip and at the outer wall, the temperature is handled with an adiabatic boundary. At internal walls, such as the core wrapper or the flow shroud, a boundary condition of the third kind is applied. The condition is fulfilled, when the temperature gradients and the temperatures on either side of the wall point shared by the two domains are equal.

Configurations

Previous calculations showed that conjugate heat transfer is a large contributor to the flow and temperature distribution in the design [16]. Additionally, we showed that partially blocking the inlet to the hot leg channeled more flow through the core, which resulted in better core temperatures. However, the flow velocity was

dramatically reduced below the design mass flow of about 32kg/s [3] and conjugate heat transfer through the flow shroud reduced the achievable temperature difference between the thermal centers of the core and the heat exchangers, in turn reducing the pressure drop that could be achieved. Through different configurations, these two problems should be mitigated.

The five different configurations which are investigated are shown in Table 1. The slit width mentioned in that table regulates the bypass flow and indicates how much larger the inlet to the hot leg is compared to the hexagonal shape of the core. A slit width of 3mm, such as in case 2, indicates that the inlet to the hot leg is a hexagonal shape with a flat-to-flat distance of 6mm larger than the hexagonal area formed by the core (≈ 16.2cm). The TBC determines how large the heat leakage is. In cases 3 to 5, a 600-µm Zircona-based TBC is applied.

Table 1: Configurations for computations.

Case	Slit width [mm]	TBC
1	Fully blocked	no
2	3	no
3	3	yes
4	13	yes
5	8	yes

All configurations were run until steady state was achieved, which was monitored through different variables such as temperature differences, max/min temperatures, pressure drops and mass flows in different parts of the geometry.

Results

ELECTRA was coarsely designed with specific design parameters in mind [3]. These postulated that the temperature difference between the thermal centers should be about 100K (ΔT_{HX}), an overall mass flow of about 32kg/s and that the distance between the thermal centers is 2.1m. The latter is a geometric constraint, which leads to a very small foot print of the reactor and it should be avoided to be changed. The other parameters are system constraints meant to keep the temperatures in the reactor in a safe operating envelope.

In this investigation, we varied two different parameters. First we introduced a thermal barrier coating which was supposed to take care of the problem of thermal leakage between the hot and cold leg. The second parameter, introduction of a by-pass flow to the core, was varied through different slit sizes which are set so that the inlet flow area to the hot leg is slightly larger than the area the core occupies, see Table 1.

Table 2: Comparison of design-critical parameters of the difference cases. Mass flows are calculated to match the full geometry. Subscripts: hl – hot leg, HX – heat exchanger, c – core

	Case 1	Case 2	Case 3	Case 4	Case 5
ΔT_{hl}[K]	123	112	122	98	107
ΔT_c[K]	207	200	192	230	194
$T_{max,c}$[K]	974	966	952	992	945
Q_{loss}[%]	40.5	36.5	27.6	22.0	24.9
Δp_{HX}[Pa]	700	810	900	1200	990
Δp_c[Pa]	1741	1518	1698	817	1346
$\dot{m}_c$[kg/s]	20.3	19	19.7	14.7	17.5
$\dot{m}_{hl}$ [kg/s]	20.5	22.5	23.5	29.5	25.6
$\dot{m}_{HX}$ [kg/s]	20.5	22.5	23.5	29.5	25.6

The results for most design critical parameters are shown in Table 2. The specification hot leg means the length difference between the plane at inlet to the hot leg at core inlet height and the plane just below the inlets of the heat exchangers. Besides the temperature and pressure differences the table also shows the heat loss, Q_{loss}, between the hot leg and cold leg as a percentage of the heating applied by the core. This is an additional indicator for the heat leakage between the channels.

The goal of this work is to decrease the maximum temperature in the core by enhancing the mass flow through the core without sacrificing the global geometric measurement, such as height and diameter of the reactor. Figure 4 shows bypass-core mass-flow ratio and the overall mass flow in relation to the maximum core temperature. In previous studies of the same geometry without inhibiting the bypass flow, the maximum core temperature rose to about 1000K, which could be traced back to the low amount of core flow [13]. In case 1, we introduced a full blockage of the bypass flow, which results in a mass flow of 20.3kg/s. The full mass flow is directed through the core, which decreases the maximum core temperature, but the full mass flow is now only about 2/3 of the design-goal mass flow. The higher flow velocities in the flow increase the pressure drop in the core and the system chokes. Introduction of a partial blockage of the bypass flow, such as in cases 2 to 5, decreases the maximum core temperature even more and simultaneously increases the overall mass flow. Even though the core mass flow decreases for all of the remaining cases, the temperature is lower for all but case 4. Some of the heat from the core is now transferred through the core wrapper to the flow passing alongside the core with the bypass flow. The only difference between cases 2 and 3 in Figure 4 is the introduction of the TBC. The difference in mass flow of these two cases is almost negligible (5% increase), however, due to fact that now a higher overall pressure drop can be achieved in case 3, more flow is channeled through the core, cooling it more effectively. By increasing the bypass flow, the overall mass flow can be increased, but a too large bypass flow will lead to less effective cooling of the

core. In case 4, the slit width and with it the bypass flow is too permissive, and the maximum core temperature is much higher than for any of the other cases, even though the system mass flow is not close to the design goal. In case 5 a good balance between bypass and core mass flow has been found. The maximum core temperature is much lower than for any of the other configuration and the system mass flow is only about 20% below the design mass flow.

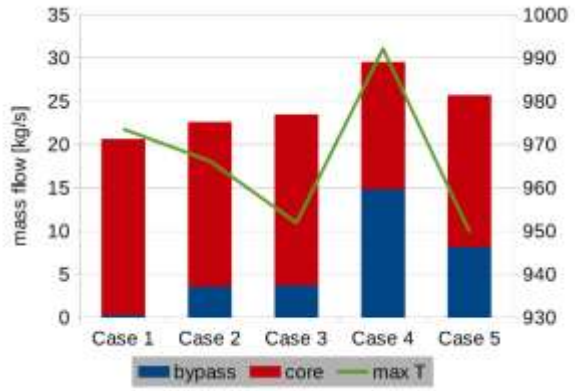

Figure 4: System mass flow ratio in relation to the maximum temperature in the core.

Figure 5 shows an overview of the temperature distribution in the reactor vessel for all 5 cases. The importance of the TBC to the thermal-hydraulic design is clearly visible from the difference in the temperature distributions. In cases 1 and 2, where no TBC is applied, wavy temperature structures are visible in the cold leg. The heat loss from the hot leg, which we quantified in

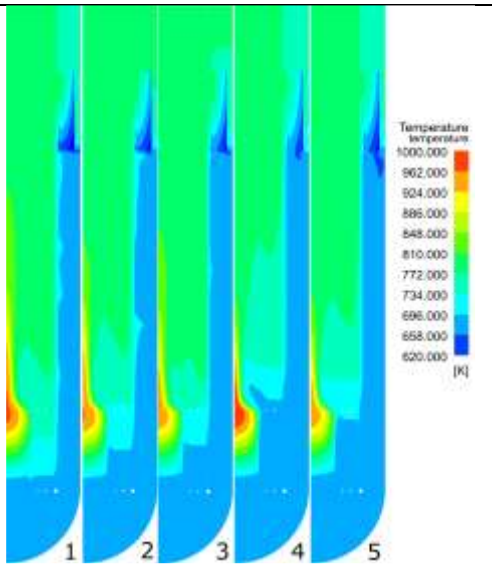

Figure 5: Comparison of the temperature distribution in the reactor for all 5 cases.

Table 2 is clearly visible in the temperature distribution. The structures become smaller and eventually invisible with the introduction of the TBC in cases 3 to 5, which is due to the reduction in heat loss from about 40.5% in case 1 down to 24.9% in case 5. Even though the heat loss in case 4 is even lower than in case 5, the maximum core temperature is much higher. In case 3, these wavy structures are still visible compared to cases 4 and 5. Additionally, the mass flow is much lower than in cases 4 and 5, which can be one of the reasons for the larger heat loss.
The residence time of the fluid in the cold leg is longer in case 3 and therefore, the fluid has more time to heat up.

Another benefit of the higher mass flow in cases 4 and 5, is the reduction of the cold zones just at the outlet of the heat exchangers. These zones, which are most pronounced in cases 1 and 2 and partly in case 3, can easily lead to freezing of the coolant in the heat exchangers in the case of transient on the secondary side. For example, if the secondary coolant is too cold or the mass flow is not regulated accordingly freezing can occur.

Comparing cases 4 and 5, it is visible that the flow in case 4 takes much longer to fully mix than in case 5, even though due to the larger velocity the turbulence levels in the former are higher. The considerably colder bypass flow in case 4 is most likely to blame. A large amount of cold fluid is transported in the bypass flow, which then cuts into the hot core flow. In case 5 on the other hand, the temperature difference between the bypass and core flow at the height of the outlet of the core is smaller, which results in a roughly 50% shorter distance until the core and the bypass flow are fully mixed compared with case 4. Figure 6 shows the velocity distribution in the reactor due to natural convection. One feature in all five distributions sticks out. A small velocity bubble right in the inside of the flow shroud in the hot leg. This elevated velocity bubble is due to the aforementioned heat transfer through the shroud. The combination of the heat lost on the hot leg side of the flow shroud and the very low velocity in the vicinity of the wall produces a falling flow in this region. This feature is undesirable, because it means that there exists a small recirculating flow within the hot leg. The introduction of the bypass flow reduces this behavior, because the upward mass flow in this region is increased (compare case 1 and 2). Another factor which plays a role in the reduction of this zone is the TBC, which we see when comparing cases 2 and 3, where the only difference is the TBC. Smaller heat transfer along the wall results in smaller negative buoyancy forces which produce the falling flow at the wall. These cannot then overcome the main flow momentum forces, and the recirculation flow is reduced.

The strong bypass flow in case 4 compared to case 5 is
clearly visible in Figure 6. Case 5, with a slit width of only 8mm, on the other hand, has larger velocities in the core, which contribute to a more effective cooling of the reactor core, decrease the maximum core temperature and therefore lead to a horizontally more evenly distributed temperature in the core (see Figure 5).

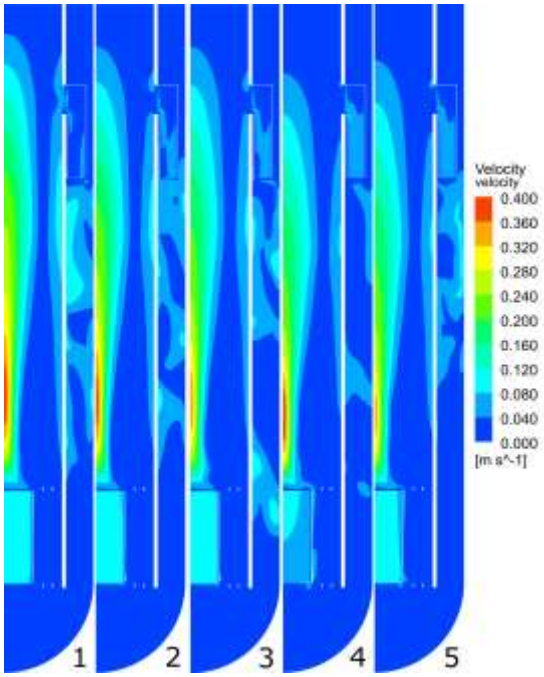

Figure 6: Comparison of the velocity distribution in the reactor for all 5 cases.

The ratio of pressure drops over the heat exchangers and the core ($\Delta p_{HX}/\Delta p_c$) is important to the maximum core temperature. Figure 7 shows this ratio together with the core-hot-leg mass flow ratio ($\dot{m}_c/\dot{m}_{hl}$) in relation to the maximum core temperature. It shows that the closer the pressure-drop-ratio is to unity, the better flow conditions with respect to minimizing the maximum core temperature can be expected. Hence, neither the heat exchangers nor the core choke the system and better flow conditions are achieved. Even though case 4 has the largest overall mass flow, the maximum core temperature is the highest of all 5 cases. The large cold bypass flow in case 4 also reduces the temperature difference over the hot leg, which results in a lower overall achievable pressure drop as described in Eq. 1. The temperature difference in case 4 is only 98K, but in case 5 this difference is 107K.

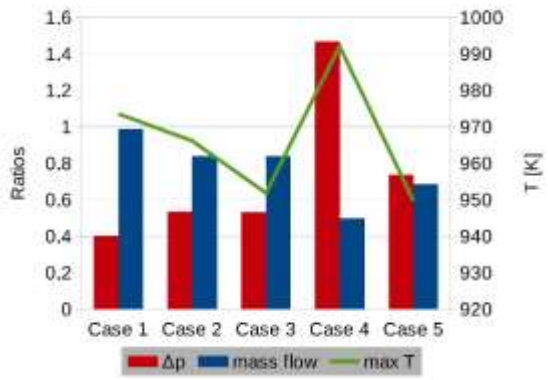

Figure 7: Ratio of the pressure drops (pHX=pc) and the mass flows (m˙ c=m˙ hl) in relation to the maximum core temperature.

Uncertainties in the final results remain, because of potential sources of error introduced during the modeling process, such as the fixed turbulent Prandtl number and the use of correlations for the heat transfer and pressure drop in the porous media domains. Despite this, the results and conclusions drawn from them should not be influenced too much. Due to the influence of the nature of semi-empirical correlations, such as the ones used in this work, the turbulent Prandtl number is largest in the wall vicinity and will influence the wall temperatures the most, but this investigation is mostly concerned with the overall mass and thermal flows within the system. The region where the results could be influenced is along the flow shroud, however, due to the very low, almost non existing, velocities in the vicinity of the flow shroud the heat transfer is dominated by conduction, which is not influenced by the turbulent Prandtl number. Due to the nature of semi-empirical correlations, such as the ones used in this work, there is always a margin of error present. Nevertheless, the correlations have been chosen based on available literature of successful similar studies in a way to minimize this uncertainty.

The accuracy of the results cannot be judged based on experimental data, because of the virtual nature of this reactor. In order to achieve credible results, the various parts of the modeling approach have been validated in previous studies [13, 14] such as the pressure drop in the HX and core (see Figure 3) and the selection of the turbulence model. Additionally, two different models have been used for the investigations. Previous studies used a full model of the reactor, while this study only uses 1/4 of the reactor, albeit, with approximately the same amount of cells. The 4.9-times increase in cell count showed no significant change in design-critical parameters (ΔT_c changed from 208K to 207K in Case 1, for which different computations exist.).

Conclusions

Calculations towards the thermal-hydraulic design of a small lead-cooled training reactor based on the ELECTRA concept have been performed with the goal of improving on previously performed calculations which showed off weaknesses in the thermal-hydraulic design. The core and the heat exchanger have been modeled with a porous-media approach. A full conjugate heat-transfer approach has been taken, because the influence of the heat loss from the hot leg through the flow shroud has a significant influence on the flow path and overall thermal hydraulic performance of the reactor. We varied two different parameters for the computations. At first a thermal barrier coating was introduced in order to decrease thermal leakage. The second parameter is a slit width which regulates the amount of allowed bypass flow. By adjusting the inlet flow area next to the core with this slit width, the bypass flow was changed between 0% and 50% of the overall flow.

The results show that varying the bypass flow has the largest influence on the design critical parameters and is the best tool to decrease the maximum core temperature. It still has to be used with care. Too much bypass flow will negatively influence the maximum temperature

in the core. An optimum ratio of the bypass to system flow was found when the core-to-HX pressure ratio was close to unity.
Due to the larger mass flow compared to a fully blocked bypass flow, the residence time of the coolant in the cold leg was reduced, which decreases the heat leakage through the flow shroud. This effect is enhanced through the usage of a thermal barrier coating on both sides of the flow shroud, decreasing the leakage even further. All these measures lead to a decrease of the maximum core temperature and a more even temperature profile in the core. Additionally, these measures also reduce the small amount of recirculating flow due to the heat transfer through the shroud.
From the analysis it becomes clear that only with a good thermal coating of the flow shroud and an optimum slit width the design critical parameters can be reached without changing the overall geometry.

Three design changes are suggested based on this investigation:

1. The most effective way to increase the global flow rate is by changing the distance between the hot and cold center. This means changing the overall geometry. However, just a small change in length should already be enough, as the newly computed critical design parameters are close to the desired values.

2. An investigation of the feasibility of even better thermal shielding needs to be carried out. The applied TBC in this work adds about 1.2mm to the 5cm thick flow shroud. Investigations into other methods of thermal shielding, such as thermal insulation inside the shroud or even thicker TBC should be performed.

3. In order to eliminate the cold spots found during the analysis, non-uniform cooling in the heat exchangers should be considered.

Acknowledgments

The computations were performed on resources at PDC Centre for High Performance Computing (PDC-HPC).

References

[1] US-DoE, 2002. A Technology Roadmap for Generation IV Nuclear Energy Systems.

[2] Fazio, C. (Ed.), 2007. Handbook on lead-bismuth eutectic alloy and lead properties material compatibility, thermal hydraulic and technologies, 2007th Edition. OECD Nuclear Energy Agency, Issy-les-Moulineaux France.

[3] Wallenius, J., Suvdantsetseg, E., Fokau, A., 2012. ELECTRA: European Lead Cooled Training Reactor. Nuclear Technology 177 (3), 303–313.

[4] Cinotti, L., Smith, C. F., Sekimoto, H., Mansani, L., Reale, M., Sienicki, J. J., 2011. Lead-cooled system design and challenges in the frame of Generation IV International Forum. Journal of Nuclear Materials 415 (3), 245–253.

[5] Frogheri, M., Alemberti, a., Mansani, L., 2013. The Advanced Lead Fast Reactor European Demonstrator (ALFRED). In: Proceedings of the 15 the International Topical Meeting on Nuclear Reactor Thermal - Hydraulics. Pisa, Italy.

[6] Alemberti, A., Carlsson, J., Malambu, E., Orden, A., Struwe, D., Agostini, P., Monti, S., 2011. European lead fast reactor - ELSY. Nuclear Engineering and Design 241 (9), 3470–3480.

[7] Castelliti, D., Baeten, P., 2013. Myrrha / Fastef Configuration Description. In: Proceedings of the 15 the International Topical Meeting on Nuclear Reactor Thermal - Hydraulics. Pisa, Italy.

[8] Bandini, G., Meloni, P., Polidori, M., 2011. Thermal-hydraulics analyses of ELSY lead fast reactor with open square core option. Nuclear Engineering and Design 241 (4), 1165–1171.

[9] Smith, C. F., Halsey, W. G., Brown, N. W., Sienicki, J. J., Moisseytsev, A., Wade, D. C., 2008. SSTAR: The US lead-cooled fast reactor (LFR). Journal of Nuclear Materials 376 (3), 255–259

[10] Abderrahim, H. A., Baeten, P., De Bruyn, D., Heyse, J., Schuurmans, P., Wagemans, J., 2010. MYRRHA, a Multipurpose hybrid Research Reactor for High-end Applications. Nuclear Physics News 20 (1), 24–28.

[11] Vanderhaegen, M., Vierendeels, J., Arien, B., 2011. CFD analysis of the MYRRHA primary cooling system. Nuclear Engineering and Design 241 (3), 775–784.

[12] Abanades, A., Pena, A., 2009. Steady-state natural circulation analysis with˜ computational fluid dynamic codes of a liquid metal-cooled accelerator driven system. Nuclear Engineering and Design 239 (2), 418–424.

[13] Shibahara, M., Takata, T., Yamaguchi, A., 2013. Numerical study on thermal stratification phenomena in upper plenum of LMFBR "MONJU". Nuclear Engineering and Design 258, 226–234.

[14] Suvdantsetseg, E., 2014. Neutronics and Transient Analysis of a Small Fast Reactor Cooled with Natural Circulation of Lead. PhD thesis, KTH Royal Institute of Technology.

[15] Author, 2013. Title. In: Proceedings. Location.

[16] Author, 2014. Title. In: Proceedings. Location.

[17] Sha, W. T., 1980. An overview on rod-bundle thermal-hydraulic analysis. Nuclear Engineering and Design 62 (1-3), 1–24.

[18] Ansys, 2014. CFX Solver Theory Guide, vers. 15. URL http://www.ansys.com

[19] Padture, N. P., Gell, M., Jordan, E. H., 2002. Thermal barrier coatings for gas turbine engine applications. Science (New York, N.Y.) 296 (5566), 280–284.

[20] Vaßen, R., Jarligo, M. O., Steinke, T., Mack, D. E., Stover, D., 2010. Overview¨ on advanced thermal barrier coatings. Surface and Coatings Technology 205 (4), 938–942.

[21] Bird, R. B., Stewart, W. E., Lightfoot, E. N., 2013. Transport Phenomena, 2nd Edition. Wiley.

[22] Menter, F. R., Kuntz, M., Langtry, R., 2003. Ten Years of Experience with the SST Turbulence Model. In: Proceedings of 4th International Symposium on Turbulence, Heat and Mass Transfer. Vol. 4. Begell House, Inc., Antalya, Turkey, pp. 625–632.

[23] Smirnov, P. E., Menter, F. R., 2009. Sensitization of the SST Turbulence Model to Rotation and Curvature by Applying the SpalartShur Correction Term. Journal of Turbomachinery 131 (4), 041010.

[24] Grotzbach, G., 2007. Anisotropy and Buoyancy in Nuclear Turbulent Heat¨ Transfer Critical Assessment and Needs for Modelling. Tech. rep., Institut fur Kern- und Energietechnik.¨

[25] Chen, F., Cai, J., Li, X., Huai, X., Wang, Y., 2014. 3D numerical simulation of fluid-solid coupled heat transfer with variable property in an LBE-helium heat exchanger. Nuclear Engineering

and Design 274, 66–76.

[26] Leibowitz, L., Blomquist, R. a., 1988. Thermal conductivity and thermal expansion of stainless steels D9 and HT9. International Journal of Thermophysics 9 (5), 873–883.

[27] Nield, D., Bejan, A., 2006. Convection in porous media, 3rd Edition. Springer Science + Business Media Inc., New York, USA.

[28] Mikityuk, K., 2009. Heat transfer to liquid metal: Review of data and correlations for tube bundles. Nuclear Engineering and Design 239 (4), 680–687. Nield, D., Bejan, A., 2006. Convection in porous media, 3rd Edition. Springer Science + Business Media Inc., New York, USA.

[29] Suvdantsetseg, E., Wallenius, J., Bortot, S., 2012. Optimization of the reactivity control drum system of ELECTRA. Nuclear Engineering and Design 252, 209–214

[30] Rehme, K., Feb. 1968. Systematische experimentelle Untersuchung der Abhangigkeit des Druckverlustes von der geometrischen Anordnung f¨ ur¨ langs durchstr¨ omte Stabb¨ undel mit Spiraldrahtabstandshaltern. Tech. rep., ¨ Gesellschaft f. Kernforschung mbH, Karlsruhe, Germany.

[31] Bubelis, E., Schikorr, M., 2008. Review and proposal for best fit of wire wrapped fuel bundle friction factor and pressure drop predictions using various existing correlations. Nuclear Engineering and Design 238 (12), 3299– 3320.